




Experimental Investigation on Dynamic Characteristics Changes of Fire Exposed Reinforced Concrete and Steel Members

Ahmet Can Altunişik ^{*}, Yunus Emrahan Akbulut, Hasan Basri Başağa and Sara Mostofi, Department of Civil Engineering, Karadeniz Technical University, 61080 Trabzon, Turkey

Ayman Mosallam and Louai F. Wafa, Civil and Environmental Engineering, The Henry Samueli School of Engineering, University of California, Irvine, USA

Received: 23 January 2021/**Accepted:** 21 October 2021/**Published online:** 5 November 2021

Abstract. Damages to structures may occur due to construction defects during various stages such as design, construction, and operation phases, or due to natural disasters during their lifetime. The Operational Modal Analysis (OMA) method enables engineers to experimentally determine the changes in dynamic characteristics of the structures that resulted from these undesirable incidents. This method can also help to estimate the structural damages and determine the usage situations depending on stiffness changes. Fire is one of the most important effects that can cause changes in dynamic behavior of structures. Considering the damages caused by fire disasters in recent years, there is a crucial need to address the effects of high temperature on the relevant field of study. This study experimentally examined the effects of elevated temperature on changes in dynamic characteristics of reinforced concrete (RC) and steel structural members. In this regard, a total of 14 (10 columns and 4 frames) laboratory models are built. These models have been constructed with various cross-sectional dimensions considering furnace dimensions. The models have undergone high temperature tests based on ISO 834 standard fire curve. Ambient vibration measurements are conducted to identify and compare the experimental dynamic characteristics both before and after fire exposure. The results show that the damages caused by high temperature significantly affect the dynamic characteristics. Damping ratios generally show a tendency to increase and some minor alterations have been observed in the mode shapes. After the fire the natural frequencies of the models have decreased. It is also observed that increases in the cross-sectional area of RC elements are an effective parameter on these decreases. The use of steel bars affects the dynamic characteristics and temperature distribution within their sections. Besides, different types of steel profiles have an effect on deformations caused by high temperatures.

Keywords: Ambient vibration measurement, Column, Damage, Dynamic characteristics, Elevated temperature, Fire, Frame, Operational modal analysis, Reinforced concrete, Steel

*Correspondence should be addressed to: Ahmet Can Altunişik, E-mail: ahmetcan@ktu.edu.tr



1. Introduction

Precise and detailed assessments of structures exposed to fire play a critical role in risk mitigation for both people and property. Achieving higher accuracy in structural modeling and evaluation directly results in higher efficiency. This consequently results in more saving of up-front investment expenses caused by factors such as material selection, protection method, and sizing.

The temperature rise, as the result of fire incidents, causes considerable changes in physical and chemical substances of various materials. Concrete and steel are considered as two of the most preferred building materials and are widely used in today's construction sector. Reinforced concrete and steel structures might experience fire hazards and be subjected to elevated temperature during their lifetime and lose their strength significantly. In this situation, by reaching the temperature to a certain value, the steel structure which has high strength and ductility at room temperature experiences a sudden loss of stability and structural collapse might occur. On the other hand, exposing RC structures to fire causes some decrease in compressive strength of concrete and loss of reinforcements strength dependent on concrete covering. The occurrence of these losses leads to severe damages, weakening, and failure of load-bearing members. This situation highlights the importance of conducting post fire evaluation for RC and steel structures and investigate their structural behavior after being exposed to high temperatures. If the fire exposed structure does not collapse, determining the structural damage level and the decision on continuing the use of the structure become crucial [1]. A considerable amount of studies has used numerical methods to evaluate fire damaged structures from different points of view [2–20].

To better understand the fire behavior of structures, it is also important to experimentally simulate the fire effects and obtain more realistic results. In this context, performing destructive and non-destructive experimental studies in field and in laboratories has started to become of interest. Conducting a full-scale fire test under a fire situation is considered a very expensive test, which only a few numbers of studies have made such expensive experience [21–25]. Besides, in these full-scale experiments, the number of tests cannot be easily increased, and maintaining the correct continuity of adjacent elements as well as forming the required support conditions in test furnace might cause some difficulties. Therefore, in response to the need for performing replication of experimental furnace test and facilitating the experimental procedure, many studies are conducting the laboratory test over a single structural member at the scaled level. The result can easily be interpreted for the full scale and simultaneously, a close to real fire scenario on the test specimen can be achieved.

The improvements of fire resistance of columns and frames have a major contribution towards the overall durability of the building under fire. Therefore, this study experimentally investigates the effects of fire on changes in dynamic characteristics of columns and frames. There exist a considerable number of studies, which experimentally evaluated the fire behavior of steel columns [26–29], as well as experimental evaluation RC columns under the fire load to evaluate [30–33].

Although there are some other related studies on mechanical characteristics of RC columns under fire, the literature lacks when it comes to experimental studies on changes in dynamic characteristics of steel and RC columns. Most of the studies on RC and steel frames are also focusing on the mechanical properties of these members under the elevated temperature [34–37]. These studies are focusing on only the mechanical properties of columns and frame systems under fire without considering the changes in dynamic characteristics.

There is comparatively less number of studies focusing on the temperature effects on dynamic characteristics changes [38–43]. Patil and Ramgir [44] have performed structural and modal analyses on carbon steel members under thermal load. The study has details on both experimental and numerical procedures. However, the analysis lacks satisfactory elaborations on how high temperature has affected the dynamic characteristics of structural members. Therefore, the present study has focused on assessing the effects of elevated temperature on dynamic characteristics of RC and steel structural members. Ambient vibration measurements are conducted to identify and compare the experimental dynamic characteristics both before and after fire exposure. Five different tests with respect to ISO 834 [45] fire curve have been conducted on constructed columns and portal frames. Based on the obtained results, the effects of fire on changes in dynamic characteristics of RC and steel columns and frame systems have been examined. The descriptions of these models are detailed in Sect. 3.1 of this paper.

2. Material Properties at Elevated Temperature

As engineering structures are exposed to fire, they experience some losses in their mass, strength, and stiffness, which can result in significant damages. Concrete is generally considered a material with low thermal conductivity and adequate behavior in fire events. However, each of the constitutive elements of concrete has different behavior in high temperatures, which affects the overall behavior of concrete in the fire. Most of the concrete volume is filled with aggregates (65% to 75%), thus the type of aggregate used in concrete mix has major effect on the behavior of concrete in high temperatures [46]. When the concrete is exposed to high temperature, aggregates expand, the water inside the concrete starts to evaporate and cement paste shrinks which form the micro cracking on the concrete surface. As the temperature goes beyond 500 °C, aggregates deteriorate which is highly dependent on type of the used aggregate [47, 48]. If the water does not evaporate from these micro cracks and the pressure inside the concrete grows more than its tensile strength, materials from surface of concrete will spall. This unfavorable phenomenon is dependent on factors such as type of aggregates and the amount of moisture content [47]. Additionally, the thermal conductivity of concrete, which has a wide range of variations, is dependent on the type of the used aggregate in the concrete mix. In this study, concrete containing the basalt stone has been used in construction of the concrete models. The water evaporation inside the concrete affects the reduction in weight of concrete. The results of the available experimental studies demonstrate that the temperature changes have

no significant effect on specific gravity of steel [47]. The density of steel is 7850 kg/m³.

The amount of moisture content plays an important role in the changes in specific heat capacity of concrete. When the water inside the concrete starts to evaporate (100 °C), the specific heat of the concrete reaches a peak value which is dependent on the amount of moisture content [47]. As for the steel, the specific heat of the carbon steel reaches its peak value at temperature of 735 °C [49]. This situation arises from the metallurgical phase change in the steel that is caused by elevated temperature [50]. The coefficient of thermal conductivity for carbon steel decreases up to 800 °C and takes a constant value for temperatures beyond 800 °C [47]. Reinforcing steel also behaves in the same manner. The modulus of elasticity, as a measure of stiffness or resistance to deformation, plays an important role in structural behavior and is significantly affected by high temperatures. When the concrete is exposed to high temperatures, its modulus of elasticity has similar behavior to its strength [51]. As for the steel, for heating rates between 2–50 °C/min, the stress–strain relationship provided in EN 1993–1-2 [49] can be used to obtain the strength and deformation properties of the carbon steel at elevated temperatures. As the temperature increases, the slope of the linear elastic region of the stress–strain relationship of carbon steel decreases.

3. Methodology

To evaluate the effects of fire on changes in dynamic characteristics, an experimental study comprising 4 main stages has been conducted. These stages are as follows: 1) constructing laboratory models, 2) ambient vibration test of undamaged models, 3) fire exposure and temperature measurements, 4) ambient vibration test of damaged models. After completing these stages, the results were evaluated and discussed. The mentioned procedures are detailed in the following sections.

3.1. Laboratory Models

The RC and steel columns and portal frames have been constructed in the laboratory to conduct non-destructive experimental measurements and evaluate the effects of fire on their behavior. Sections of the models have been selected in accordance with furnace dimensions and each of them having an RC foundation with 20 cm thickness. To construct the models, grade 50/60 concrete was used. The models are placed on the car-bottom of the test furnace, and they should have a minimum distance of 30 cm from heating elements and furnace ceiling. All models had an equal height of 1.5 m above their foundations. A clear cover of 25 mm and steel rebar with 8 mm diameter have been used for all RC models. In this study, reinforcements of RC frame configurations are non-seismically detailed. Steel columns and frames have been constructed using unprotected steel profiles painted after the sandblasting process. Figure 1 shows some views of the RC and steel laboratory models.



Figure 1. Some views of the RC and steel laboratory models.

While molding the concrete models, standard cylindrical and cube samples have been cast to determine the material properties. Here, a total of six cube samples (150×150 mm) and three cylinder samples (100×200 mm) have been tested. The curing process, which is required to control the moisture losses after the manufacturing of the models and to ensure proper and timely hydration reactions, has been done by watering the concrete surfaces for 7 days. As the result of these tests, the density was calculated as 2530 kg/m^3 . Also, the dynamic and static elasticity modulus of concrete on the 85th day were calculated as 38,320 MPa and 29,933 MPa, respectively. It was determined that average concrete strength is 50 MPa.

3.1.1. RC Columns and Frames To perform the required experimental tests, four RC models have been constructed in the laboratory.

- It is generally known that dimensions of structural elements play an important role in stiffness. As the size of element increases, stiffness of the element also increases. In this regard, the effects of dimensions on the results have been evaluated using six columns with different cross-sectional sizes. These columns have been constructed on a single foundation with a minimum distance of 30 cm from each other.
- Two RC frame models, having same geometry have been constructed. The frame models are constructed with one-bay, one-story and all elements of each frame configuration are having same cross-sectional dimensions. A preliminary test has been conducted on one of the frame models and its feedbacks have been used to perform the actual tests more precisely.
- To assess the effects of steel reinforcements on dynamic characteristics and temperature distributions, two columns having same cross-sectional dimensions have been constructed with and without reinforcement bars.

Figure 2 shows the geometrical configuration and reinforcement details of RC columns and frames. During the pouring procedure, temperature measurement stations have been positioned within certain intervals on RC models. For later

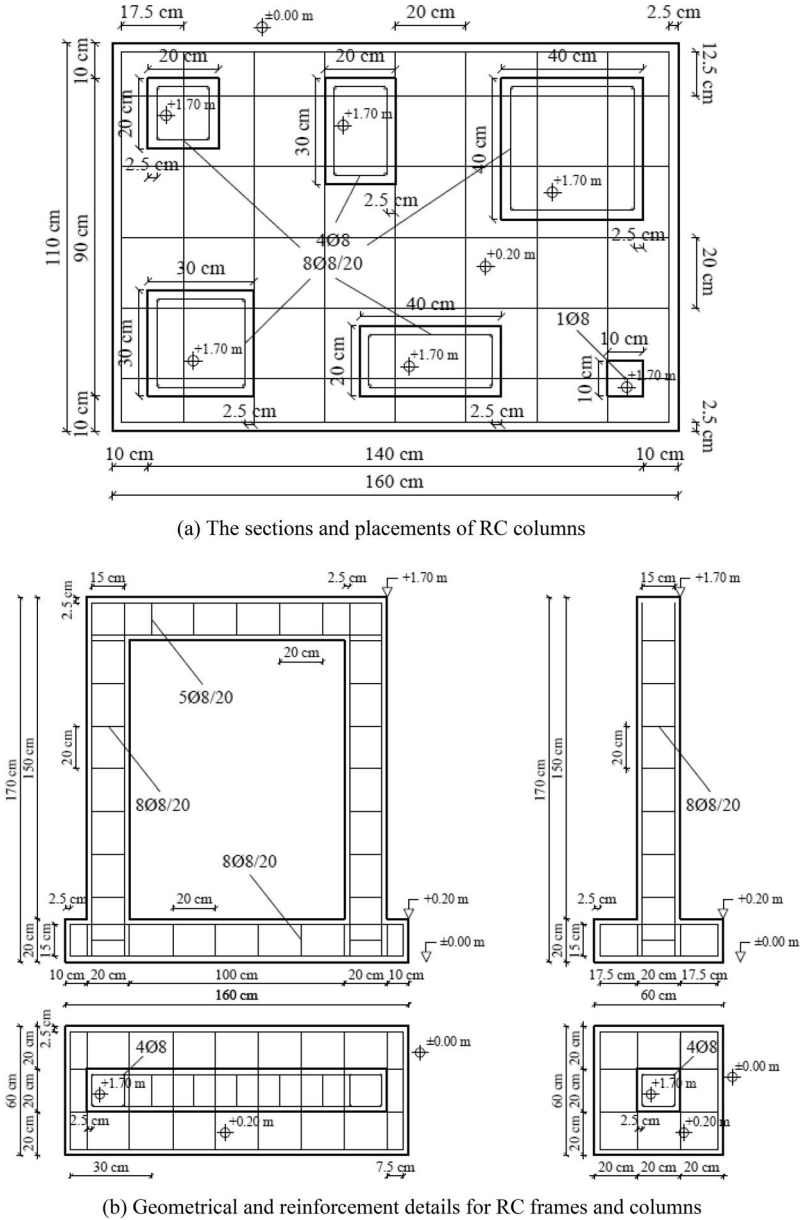


Figure 2. The geometrical configuration and reinforcement details of RC columns and frames. a The sections and placements of RC columns. b Geometrical and reinforcement details for RC frames and columns.

placement of thermocouples, one-way open-end pipe covers were embedded in designated measurement stations. This is to record sectional temperature changes at measurement stations. Utilized protective pipe covers are manufactured with

AISI 310 stainless steel. The pipe covers dimensions were $2 \times 6 \times 70$ mm and $2 \times 6 \times 120$ mm (thickness, outer diameter, pipe length). To use the thermocouples again and prevent possible damages, these protective pipes were used. As using these covers might affect the measured values, drilled measurement stations were also designated at locations similar to the pipe covers to improve the measurement accuracy. The thermocouples are to be embedded in full contact with the end of the protective covers and the drilled holes. The details of the temperature measurements are presented in Sect. 3.2.

3.1.2. Steel Columns and Frames In this study, a total of four steel models, comprising of two portal frames and two columns, have been constructed. To evaluate the effects of profile types on the results, models were built using two different steel profiles.

- The frame specimens consist of one-bay and one-story. One frame was built up using HEA and the other used SHS profile. The beam and columns of each frame consist of the same profile.
- HEA and SHS profile types have been used to fabricate the column specimens.

As for the column-beam joints, welded joints and joint connector bolts have been used for the SHS frame and HEA frame, respectively. The beam and columns of the HEA frame are connected using 4 pieces of M16 bolts and a plate having a thickness of 10 mm. The columns were welded to the base plate ($340 \times 340 \times 10$ mm) on top of their foundation and completely tightened to the foundation using 4 anchor bolts (M20). Figures 3 and 4 present the geometrical properties and connection details of steel columns and frames.

3.2. Fire Exposure and Temperature Measurements

The required fire tests have been carried out using a custom designed car-bottom annealing furnace. The movement of the car-bottom of the furnace is through a gearmotor. The properties and general view of the test furnace are illustrated in Table 1 and Fig. 5.

There exist two K-type thermocouples embedded in the ceiling of the furnace. Each thermocouple is attached to a control device placed on the electrical distribution panel of the furnace. One temperature controller has been used to define the time–temperature relationship according to ISO 834 fire curve, while the other has been used to define the maximum limit of temperature for safety purposes. Heating elements are located on three sides of the furnace. The sections having less distance to the sidewall experience more heating during the tests. To be able to compare the measured temperatures, it was tried to place the models on the furnace car-bottom as symmetrical as possible. To simulate the effect of fire on the models, ISO 834 standard fire curve has been selected as the time–temperature relationship. All tests have been performed for an exposure duration of 3 h.

To determine the temperature changes occurring within sections and on surfaces, a pyrometer, thermocouples, paperless recorder and OPR500 Data-Viewer

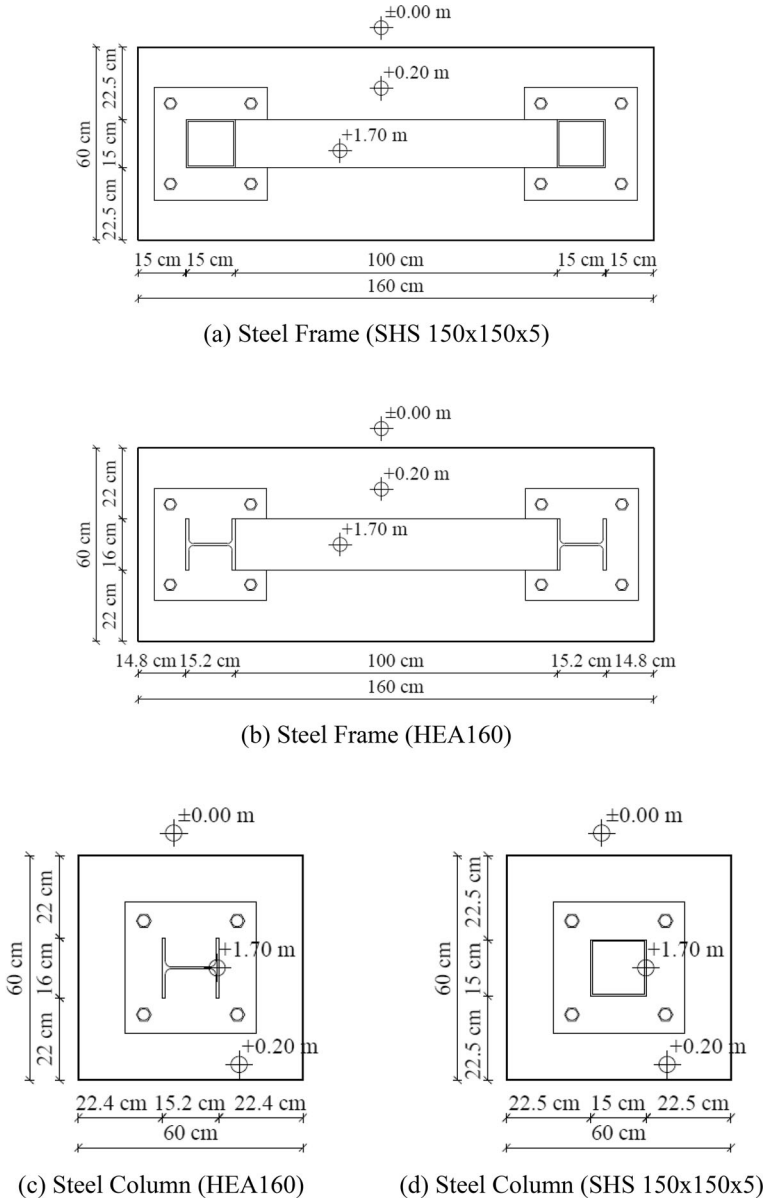


Figure 3. Geometrical configuration of steel frames and columns. a Steel Frame (SHS 150 × 150x5) b Steel Frame (HEA160). c Steel Column (HEA160) d Steel Column (SHS 150 × 150x5).

software have been used. The unprotected steel has high thermal conductivity, so there will be no significant differences in temperature distributions within sections of these elements. Therefore, no thermocouple was embedded on steel models and

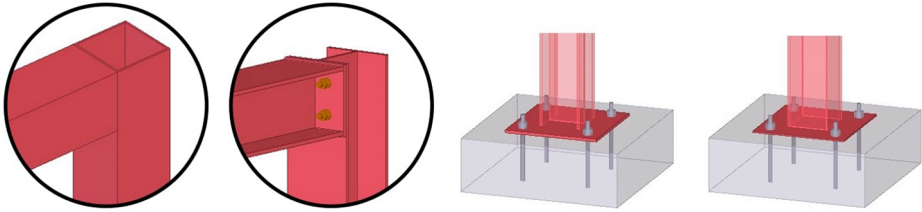


Figure 4. Connection details of steel frames and columns.

**Table 1
General Information of Utilized Test Furnace**

Type	Car-bottom annealing furnace
Chamber size	2000 × 1500 × 2000 (W x L x H) mm
Operating temperature	1100 °C
Maximum temperature	1120 °C
Heated by	Electricity
Heating power	210 kW



Figure 5. Car-bottom annealing furnace.

their temperature measurements only involved measuring the surface temperatures of the elements. A dual laser AST TI 1500 portable pyrometer has been used to measure the surface temperatures. In each test on RC models, a total of 10 thermocouples were placed in allocated measurement stations to measure the temperature development within the section of the models during exposure duration. OPR500 paperless recorder has been used to monitor and record temperature changes.

The overall procedures for the fire exposure and temperature measurements, conducted in this study, are as follows:

(The steps marked with an asterisk (*) have been performed for RC models only.)

1. Placing the constructed specimens on the car-bottom of the furnace
2. Locating the thermocouples in temperature measurement stations and connecting each thermocouple to its relevant channel on paperless recording device *
3. Determining the surface temperatures of the specimens before being exposed to fire
4. Defining ISO 834 curve in step controller of the furnace
5. Definition of maximum temperature value (1150 °C) using the other controller device for safety purposes
6. Exposing the test specimens to fire for 3 h
7. Monitoring and recording the interior temperature of the furnace during the tests
8. Determining the surface temperatures of the specimens after being exposed to fire
9. Placing the specimens outside the furnace to cool down and adjust their temperature with the room ambient temperature
10. Employing a paperless recorder to collect the data from each of the thermocouples, transfer them to the computer, and visualizing the collected real-time data in form of graphs to represent the temperature variation over time *

With respect to these steps, five high temperature tests (Test 1–5) have been done. The developments in furnace interior temperature during the tests, along with the defined fire curve to the furnace (ISO 834) are presented in Fig. 6. Although, same time–temperature relationship and same exposure duration have been considered in all tests, the volumes, and masses of the models inside the fur-

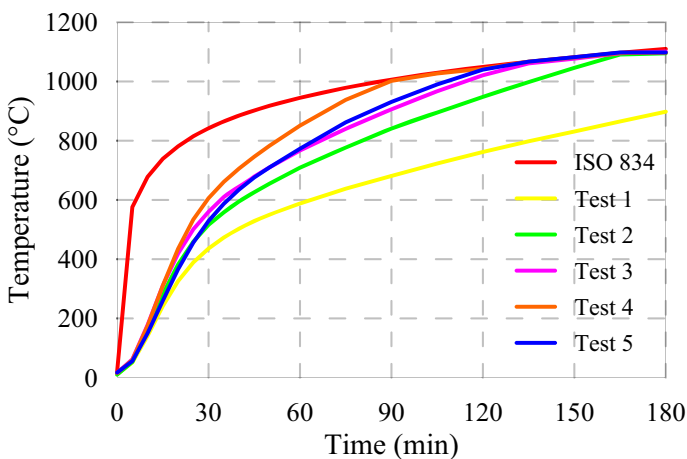


Figure 6. Furnace interior temperature developments during the tests and ISO 834 fire curve.

nance are not same. So, in each test, the furnace interior temperature was increased at different rates and the obtained temperature development curve from each test was distinctive. Since the furnace has high thermal power, this uniform temperature effect was achieved in the early stages of the tests. During the fire exposure of steel models, burning of the steel profile painting generated combustible gases. After the tests are over, while opening the furnace door, these gases came in contact with oxygen and flare up again.

3.2.1. Test-1 The first test has been conducted on an RC specimen comprising of six columns having different cross-sectional sizes. A total of ten measurement stations, nine on the columns and one in the middle of the foundation, are located in this model (Fig. 7). The measurement stations on the columns have located at a distance of 1 m (± 2 cm) from the bottom. The details of the measurement stations are demonstrated in Table 2.

In this test, after 180 min of fire exposure, the furnace interior temperature reached 898 °C (Fig. 6). The changes in temperature obtained from measurement stations, within fire exposure duration, are presented in Fig. 8. After completing the test, a temperature range of 575–600 °C has been obtained as surface temperatures of the columns. The steps of the performed test are shown in Figs. 9 and 10.

3.2.2. Test-2 The second test has been conducted on the RC frame model comprising of beam and columns with cross-sectional dimensions of 20 × 20 cm, having ten built-in measurement stations. These stations are located in sections close to joints of column-beam and column-foundation, as well as midpoints of beam and foundation (Fig. 11). The specifications of measurement stations are presented in Table 3.

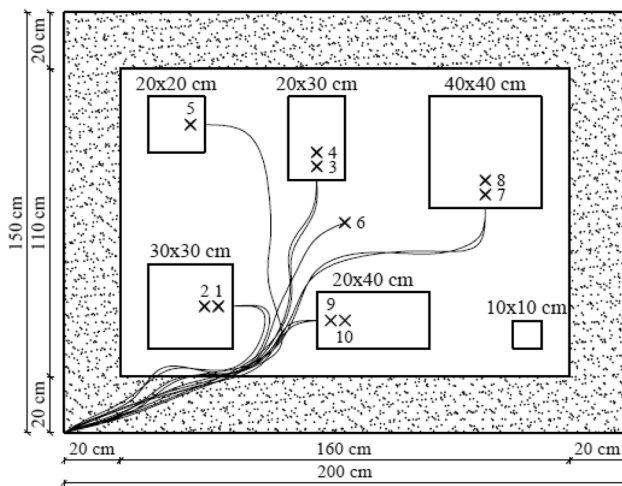


Figure 7. Schematic view of the RC columns and locations of measurement stations.

Table 2
Details of the Measurement Station

No	1	2	3	4	5	6	7	8	9	10
Depth (cm)	5.2	10.2	5.2	10.1	5.3	5.5	6.5	9.9	5.2	9.9
Protective cover	✓	✓	✓	✓	✓	✓	✗	✗	✓	✓

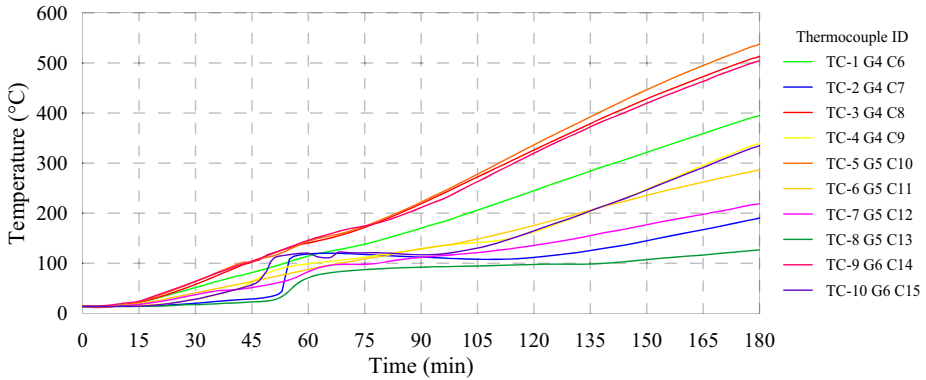


Figure 8. Temperature variations during Test-1.



Figure 9. Pretest state of Test-1.

The interior temperature of the furnace has reached to value of 1095 °C after 180 min of fire exposure (Fig. 6). The variations in temperature of measurement stations, within test duration, are presented in Fig. 12. It is observed that the surface temperatures of the model are in the range of 715–740 °C at the end of the test. It is determined that the surface temperatures measured 1 h after the various parts of the model in the cooling stage are between 240–320 °C, and the measured surface temperatures after 3 h are between 125–190 °C. Preparation and general overview of the test are illustrated in Figs. 13 and 14.

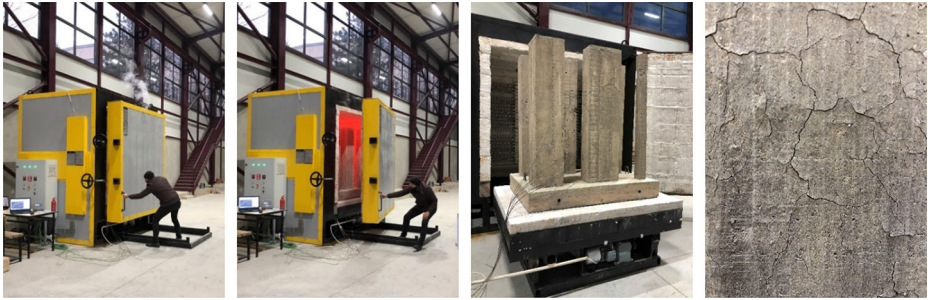


Figure 10. Posttest state of Test-1.

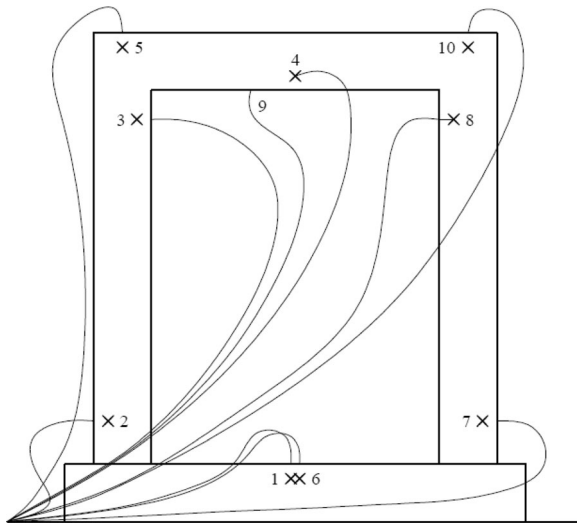


Figure 11. Schematic view of the RC frame and locations of measurement stations.

**Table 3
Descriptions of Measurement Stations**

No	1	2	3	4	5	6	7	8	9	10
Depth (cm)	4.7	5.5	5.0	5.0	5.0	5.5	5.1	5.0	4.8	5.0
Protective cover	✗	✗	✗	✗		✓	✓	✓	✓	✓

3.2.3. *Test-3* The third high temperature test has been conducted on column models. Both columns are having same cross-sectional dimensions of 20 × 20 cm, while only one of them has reinforcement bars. Five temperature stations have been formed on each of these models (Fig. 15). The measurement stations are

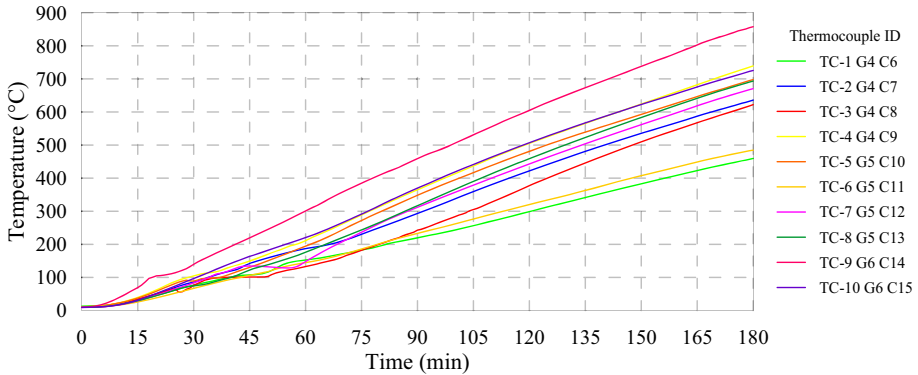


Figure 12. Temperature variations during Test-2.



Figure 13. Pretest state of Test-2.

located 1 m above the bottom of the columns (Table 4). After the 180 min exposure duration, the interior temperature of the furnace reached the value of 1101 °C (Fig. 6). The temperature changes occurred during the test are presented in Fig. 16.

Upon completion of the test, a temperature range of 760–795 °C has been observed as surface temperatures of the columns. The stages of this test are depicted in Figs. 17 and 18.

3.2.4. Test-4 To conduct the fourth test, a steel portal frame comprising a 150 × 150x5mm SHS profile assembled through a welded connection has been used. The position of the model in the furnace is presented in Fig. 19. The interior temperature of the furnace has reached the temperature value of 1097 °C after 180 min of fire exposure (Fig. 6). The surface temperature of different faces of the models showed a temperature range of 820–855 °C. The temperature measurements from various parts of the RC foundation are in the range of 650–740 °C. Figures 20 and 21 illustrate the different stages of this test.



Figure 14. Posttest state of Test-2.

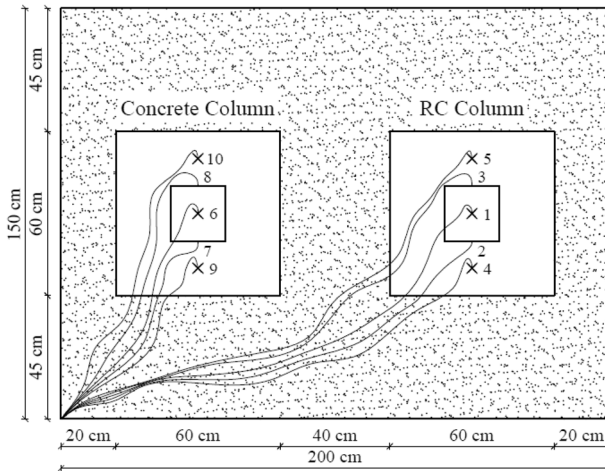


Figure 15. Schematic view of the columns and locations of measurement stations.

3.2.5. *Test-5* The fifth test is carried out using a steel portal frame and two steel columns. Frame configuration comprises HEA160 profiles assembled using bolts connections. The two constructed columns comprised HEA160 and SHS with cross-sectional dimensions of $150 \times 150 \times 5$ mm. The position of the models in the furnace is given in Fig. 22. The interior temperature reached the value of $1098 \text{ }^\circ\text{C}$

Table 4
Details of the Measurement Stations

No	1	2	3	4	5	6	7	8	9	10
Depth (cm)	5.0	5.0	5.5	5.1	5.0	5.2	5.5	5.4	5.5	5.4
Protective cover	✓	✓	✗	✓	✗	✓	✓	✗	✓	✗

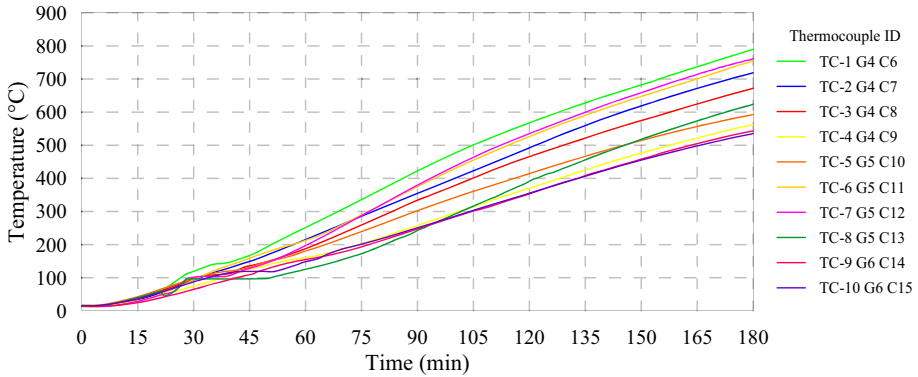


Figure 16. Temperature variations during Test-3.

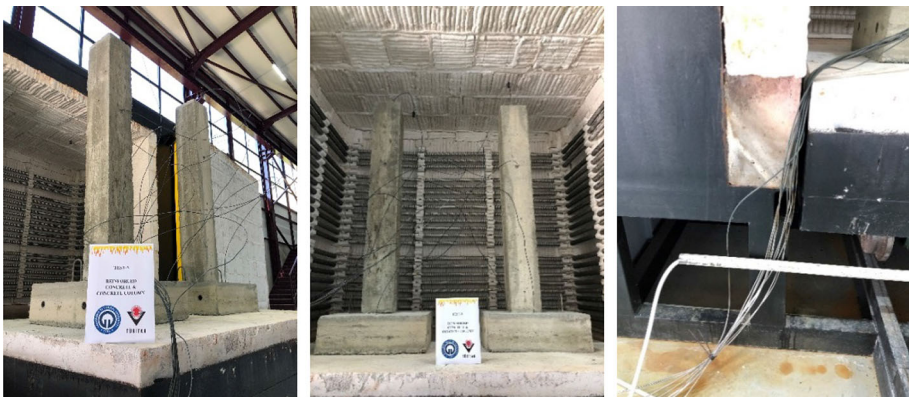


Figure 17. Pretest state of Test-3.

after completing 180 min of fire exposure (Fig. 6). After the test is over, the temperature of various locations on the surfaces is measured between 830 and 850 °C. The temperature measurements from various parts of the RC foundation are on average 740 °C. Visual overviews of this test are presented in Figs. 23 and 24.

After conducting all 5 fire exposure tests, the results obtained from each test were processed and evaluated. Then, to have a better evaluation, the findings from each fire exposure test were compared. As a result of the comparison between the

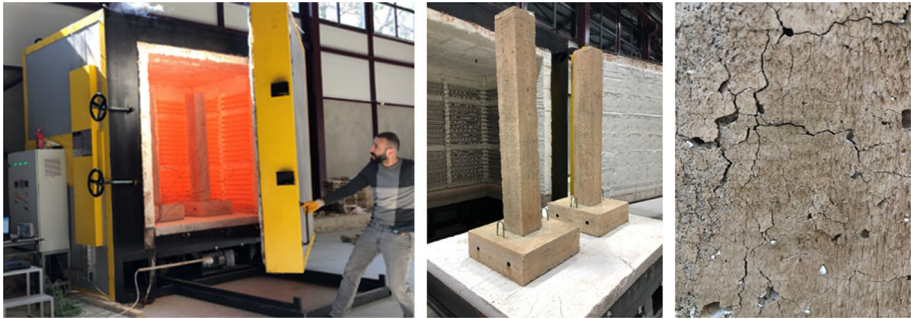


Figure 18. Posttest state of Test-3.

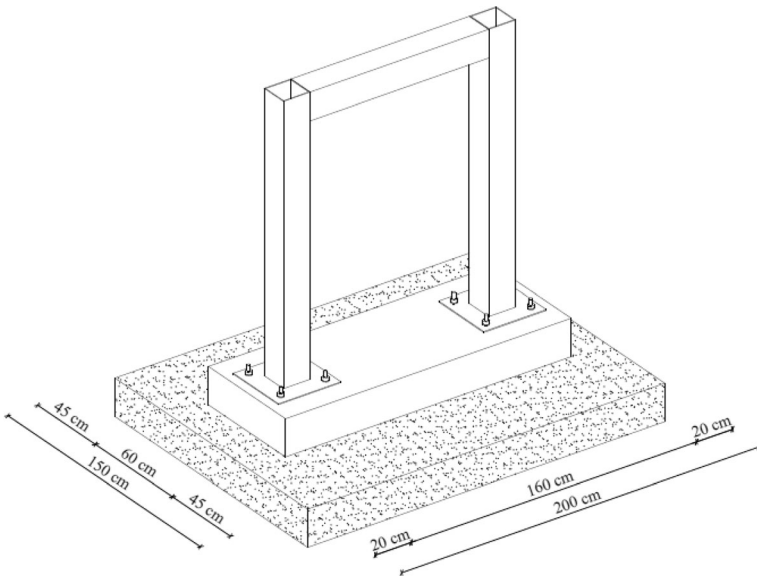


Figure 19. The location of the steel frame model consisting of SHS profile.

cross-sectional temperature values obtained from concrete and RC models, minor differences have been obtained. These differences are likely related to the formation of the measurement stations, a slight difference in the depth of the created measurement stations, distance of measurement stations from heating elements, thermocouples which might not be in full contact with the measurement stations, and thermal effects between models used in the same test. Since models are placed at different distances from heating elements during the test, temperature did not symmetrically distribute within sections of the concrete and RC elements.

In RC models, for constant exposure duration, elements with smaller cross-sectional dimensions have a faster rate of increase in their cross-sectional temperatures. As the temperature of the measurement station reached 100 °C, for a short



Figure 20. Pretest state of Test-4.

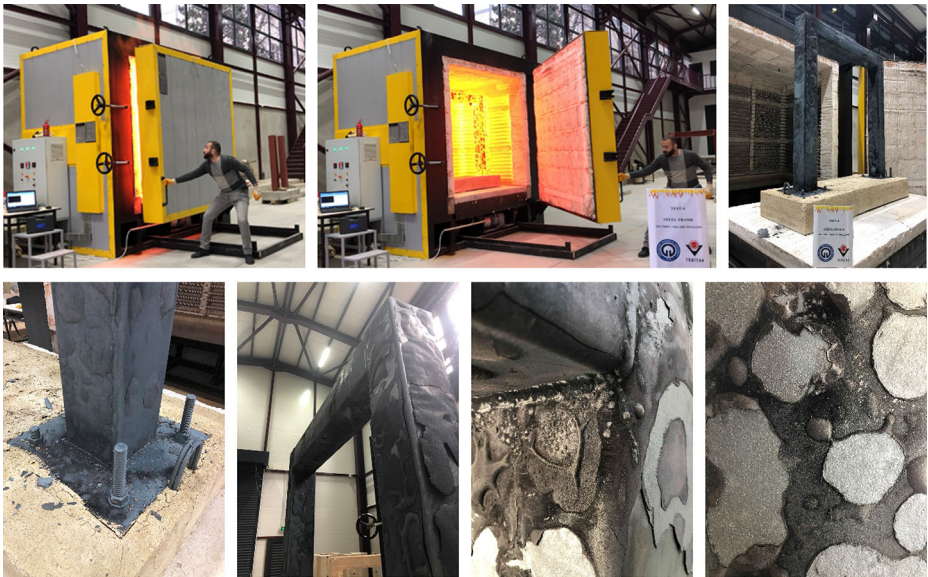


Figure 21. Posttest state of Test-4.

period temperature demonstrated different behaviors including a decrease in its rate of increase, as well as being constant and fluctuations. The reason for this behavior is that at 100 °C, concretes water evaporation occurs at a more rapid pace. Hypothetically, the temperature of the measurement stations will not increase until the water is fully evaporated. This behavior is more visible in measurement stations where thermocouples are directly placed in drilled holes.

During the tests on concrete and RC models, no serious spalling has been observed and specimens retained their initial form. However, some visible cracks

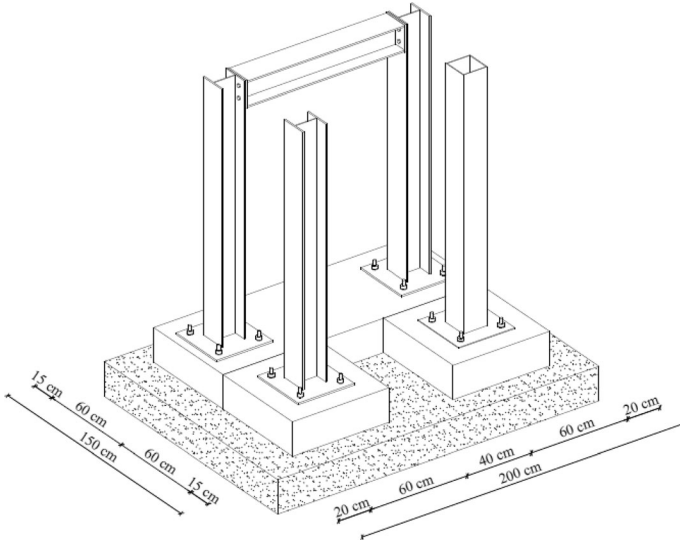


Figure 22. The location of the steel frame and columns consisting of HEA and SHS profiles.



Figure 23. Pretest state of Test-5.

appeared on the outer surfaces. In addition, having different fire scenarios caused the models to experience different changes in their colors. The results of the fire exposure of concrete and RC columns in Test-3, point out the effectiveness of reinforcing steel on temperature distribution within the section. However, this effect is not very critical (Fig. 16). In tests on steel models, the oxidation on steel surface, which occurred due to fire, was peeled off during the cool down period.



Figure 24. Posttest state of Test-5.

3.3. Evaluation of Dynamic Characteristics

There are two basically different methods available to experimentally identify the dynamic system parameters of a structure: Experimental Modal Analysis (EMA) and Operational Modal Analysis (OMA). In the EMA, the structure is excited by known input force and response of the structure is measured. In the OMA, the structure is excited by unknown input forces (ambient vibrations) and response of the structure is measured. Ambient excitations such as traffic, wave, wind, earthquake and their combination are environmental or natural excitations. Therefore, the system identification techniques through ambient vibration measurements become very attractive. In an ambient vibration test, the input force is unknown and accordingly ambient excitation is incapable of both the calculating either the Frequency Response Functions (FRFs) or the Impulse Response Functions (IRFs) of the structure. To evaluate the changes in dynamic characteristics such as natural frequency, mode shape and damping ratio, the OMA method has been used both before and after fire exposure.

The vibration data are collected by ambient vibration test and transferred to PULSE [52] and OMA [53] software for signal processing. To measure the structural vibrations of the constructed models, B&K type 4506 B 003 triaxial accelerometers have been used (Fig. 25). The sensitivity, operating frequency range and maximum acceleration value of these accelerometers were 0.5 V/g, 0.3–2000 Hz and ± 14 g, respectively. To accurately obtain the dynamic characteristics, the numbers and locations of accelerometers have been specified according to the performed modal analyses using finite element methods. These modal analyses were performed to confirm the oscillation locations. Total of 4 measurement

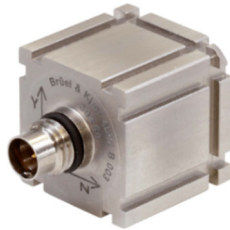


Figure 25. Triaxial accelerometer.

points are located on each model. For column specimens, one accelerometer is attached to the top and the others are located at equal distances from each other in a way that the height of the columns is divided into four equal sections. As for the frame models, these accelerometers are placed at the mid-height of the columns and the beam-column connections. In the performed ambient vibration tests, single test setup settings have been used.

In these tests, the frequency range is selected as 0-500 Hz. Measurements are carried out for 10 min. B&K 3560 type 17-channel data acquisition system is used to collect the vibration signals (Fig. 26). Various modal parameter identification techniques are available. These techniques were developed by improving both the computing capacity and signal processing procedures. Two popular techniques are frequently used to extract modal parameters; namely: (i) the Enhanced Frequency Domain Decomposition (EFDD), in the frequency-domain, and (ii) the Stochastic Subspace Identification (SSI) in the time-domain. The vibration signals are processed by using EFDD method [54]. The singular values of the spectral density matrices (SVSDM) and the average of all spectral densities (AASD) have been graphed.

The dominant frequency region around the peak is determined from the graph where the singular values of the spectral density matrix are obtained. Modal Assurance Criterion (MAC) method is used while determining the dominant frequency region. A MAC value of 100% indicates that the mode shapes are the same, while a MAC value approaching zero indicates that the mode shapes are incompatible. It is recommended that at least 95% similarity between the dominant frequency region mode shapes using the MAC method. After determining



Figure 26. Data acquisition system.

the dominant frequency region, the value with the highest signal (DB) shows the frequency of the structure. When any peak point is selected, if that point does not belong to the structural mode (can be called as false peak), the program does not complete the operation or it is directed to the peak point of the real structural mode, which is in close frequency neighborhood. The dominant frequency region is also used to calculate the damping ratios of the structure. To extract the damping ratio, logarithmic decrement method has been used. Logarithmic decrement represents the rate at which the amplitude of a free damped vibration decreases. It is defined as the natural logarithm of the ratio of any two successive amplitudes. It is found from the time response of underdamped vibration.

Ambient vibration tests have been performed before fire exposure to determine the dynamic characteristics of each model at ambient temperature (20 °C). Later, all laboratory models were subjected to fire load in the test furnace and the high temperature imposed some physical changes such as deformations and cracks on the tested specimens. After fire exposure, experimental measurements are repeated. By comparing the measured values obtained from undamaged and damaged conditions, the changes in dynamic characteristics of test specimens are evaluated. Figure 27 shows an overview of the conducted non-destructive experimental measurements.

After the fire test on concrete column (Test-3), while lowering the model from the car-bottom, the column accidentally separated from its foundation. For this reason, the dynamic characteristics of the damaged condition could not be measured. Thus, the model had excluded from the rest of the study, and only the dynamic characteristics of the undamaged condition are presented.

The SVSDM and AASD obtained from all measurements, before and after fire exposure, are presented in Fig. 28. The extracted first four mode shapes are also presented in Table 5. Since the mode shapes obtained for both the undamaged and damaged cases of the same type of models are close to each other, only the data for one model and measurement are presented. Table 6 present the natural frequencies and damping ratios of the models before and after the fire exposure. Besides, the frequency values of all models and the percentage of changes in natural frequencies and damping ratios after fire are graphically presented (Fig. 29–31).

The dynamic characteristics of the structures are depending on their mass and stiffness. The stiffness is a function of cross-sectional area and modulus of elasticity. At elevated temperatures, concrete experienced mass losses which is due to a decrease in density and spalling. Spalling reduced the cross-sectional dimensions of the fire exposed elements, resulting in a reduction in mass and stiffness. However, in the performed experiments, there was no trace of major spalling. So, the observed mass loss was due to water evaporation from concrete, and reductions in the elastic modulus of concrete resulted in reduced stiffness. In unprotected steel models, thermal strain caused residual deformations and sectional distortions. This deformation was more apparent in steel frames.

As demonstrated in the above figures and tables, the natural frequency values of the undamaged models are increasing with increases in their cross-sectional area. For models having symmetrical cross-sections, it was expected to have twin



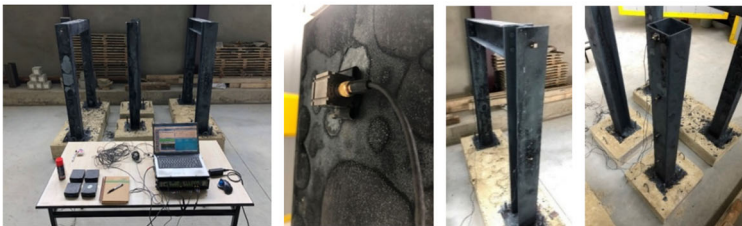
(a) Undamaged concrete and RC models



(b) Damaged concrete and RC models



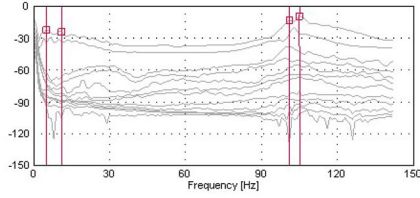
(c) Undamaged steel models



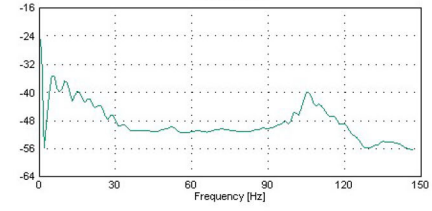
(d) Damaged steel models

Figure 27. Some views from the non-destructive experimental measurements. a Undamaged concrete and RC models b Damaged concrete and RC models c Undamaged steel models d Damaged steel models.

[dB] (1 m/s)² / Hz Enhanced Frequency Domain Decomposition - Peak Picking
Singular Values of Spectral Density Matrices
of Data Set: Measurement 1

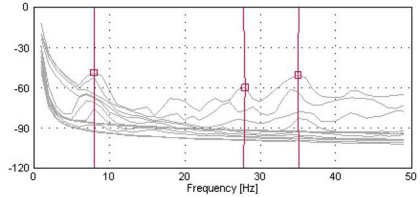


[dB] (1 m/s)² / Hz Average of All Spectral Densities of Data Set
Measurement 1

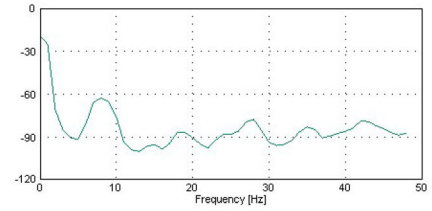


(a) Undamaged condition of RC column 10x10

[dB] (1 m/s)² / Hz Enhanced Frequency Domain Decomposition - Peak Picking
Singular Values of Spectral Density Matrices
of Data Set: Measurement 1

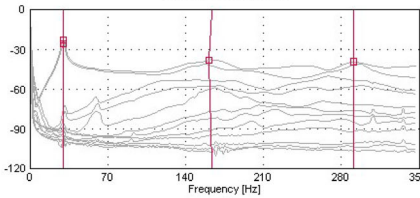


[dB] (1 m/s)² / Hz Average of All Spectral Densities of Data Set
Measurement 1

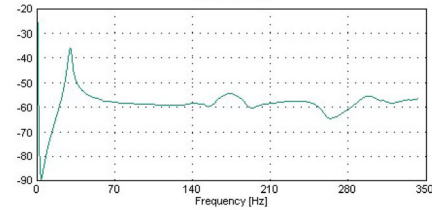


(b) Damaged condition of RC column 10x10

[dB] (1 m/s)² / Hz Enhanced Frequency Domain Decomposition - Peak Picking
Singular Values of Spectral Density Matrices
of Data Set: Measurement 1

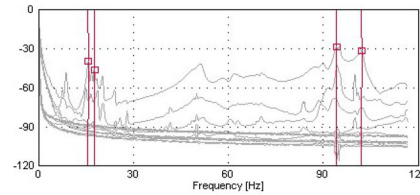


[dB] (1 m/s)² / Hz Average of All Spectral Densities of Data Set
Measurement 1

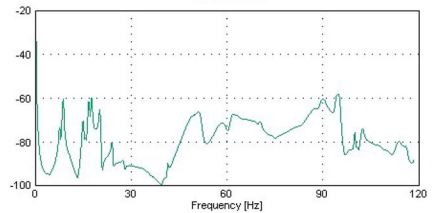


(c) Undamaged condition of RC column 20x20

[dB] (1 m/s)² / Hz Enhanced Frequency Domain Decomposition - Peak Picking
Singular Values of Spectral Density Matrices
of Data Set: Measurement 1



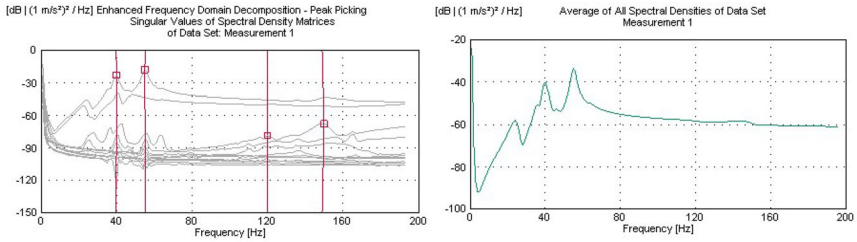
[dB] (1 m/s)² / Hz Average of All Spectral Densities of Data Set
Measurement 1



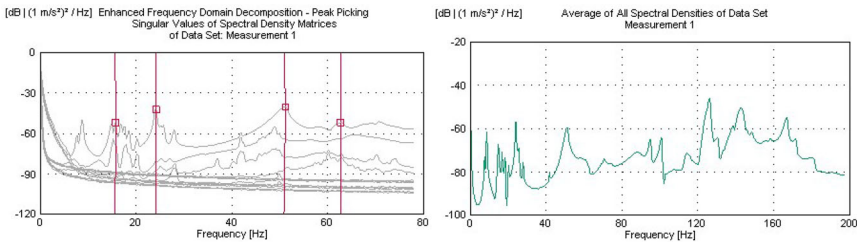
(d) Damaged condition of RC column 20x20

◀ **Figure 28. SVSDM and AASD obtained from all measurements before and after fire a Undamaged condition of RC column 10 × 10 b Damaged condition of RC column 10 × 10 c Undamaged condition of RC column 20 × 20 d Damaged condition of RC column 20 × 20 e Undamaged condition of RC column 20 × 30 f Damaged condition of RC column 20 × 30 g Undamaged condition of RC column 20 × 40 h Damaged condition of RC column 20 × 40 i Undamaged condition of RC column 30 × 30 j Damaged condition of RC column 30 × 30 k Undamaged condition of RC column 40 × 40 l Damaged condition of RC column 40 × 40 m Undamaged condition of concrete column 20 × 20 n Undamaged condition of RC frame 20 × 20 o Damaged condition of RC frame 20 × 20 p Undamaged condition of steel frame SHS 150 × 150x5 q Damaged condition of steel frame SHS 150 × 150x5 r Undamaged condition of steel frame HEA160 s Damaged condition of steel frame HEA160 t Undamaged condition of steel column HEA160 u Damaged condition of steel column HEA160 v Undamaged condition of steel column SHS 150 × 150x5 w Damaged condition of steel column SHS 150 × 150x5.**

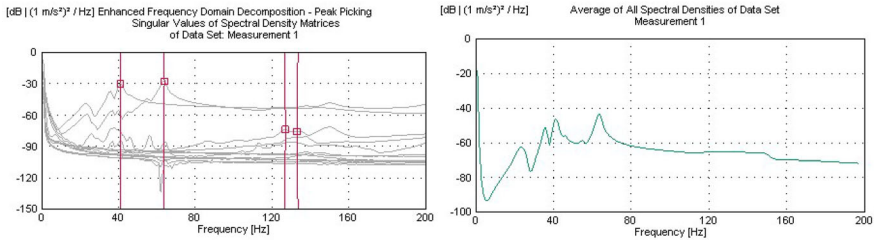
modes. However, as the results of the performed measurements it was observed that in some of these models, the natural frequency values of the twin modes were slightly different. These minor differences are associated with numerical reasons such as signal processing for OMA. It was observed that damages incurred by high temperatures decrease the natural frequency values of the models. In the RC models, the natural frequency values of the first 4 modes have experienced a change of 27%—73% compared to initial values. In the performed OMA measurements, it was observed that increases in the cross-sectional dimension of RC columns are effective on the percentage of decrease in the frequency values of these elements. Comparing the undamaged OMA measurements of two columns in Test-3 having the same geometry shows that existence of steel reinforcements in RC elements affects the dynamic characteristics. However, as the concrete column was broken, the post fire measurements could not be conducted. So, the effect of using reinforcing steel in dynamic characteristics of damaged condition could not be examined. In the steel specimens, natural frequencies of SHS models experienced more changes compared to models with HEA profiles. Comparing the results of steel columns show few if any changes in the first 4 natural frequencies of columns with HEA profile (maximum 5%), whilst the first natural frequency of the SHS column experienced a decrease of 33% compared to the initial condition. The main reason behind this variation is the deformations occurring in elements cross-section of SHS profile. Assessing the results obtained from steel frames, it can be seen that profile type can affect the natural frequency values. The first two natural frequency values of the frame model consist of HEA profile connecting with a bolt connection, did not change (maximum 3%), but the frame model with SHS profile and welded connection experienced 20% and 30% of changes in natural frequency values of its first two modes, respectively. The main reason behind



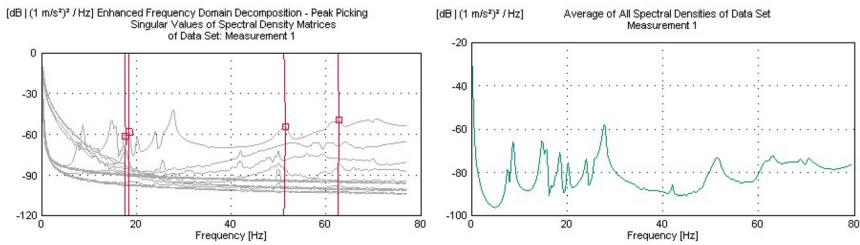
(e) Undamaged condition of RC column 20x30



(f) Damaged condition of RC column 20x30

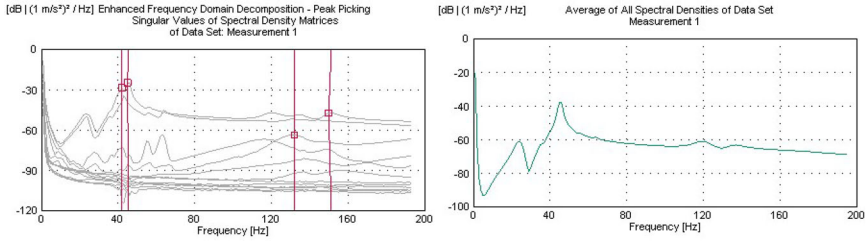


(g) Undamaged condition of RC column 20x40

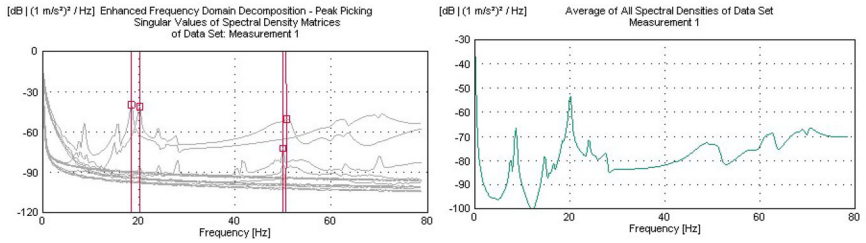


(h) Damaged condition of RC column 20x40

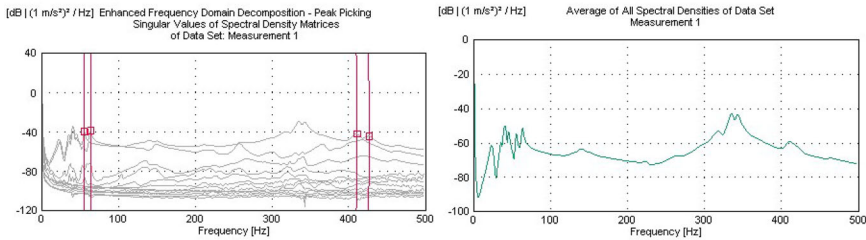
Figure 28. continued.



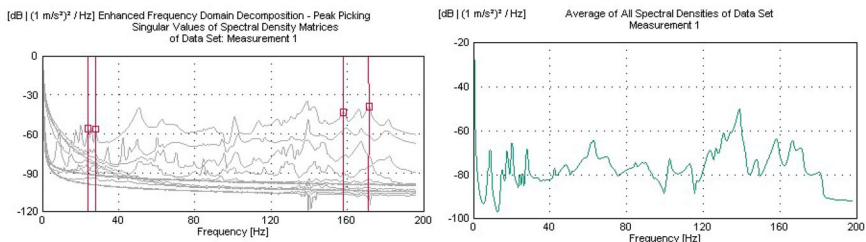
(i) Undamaged condition of RC column 30x30



(j) Damaged condition of RC column 30x30

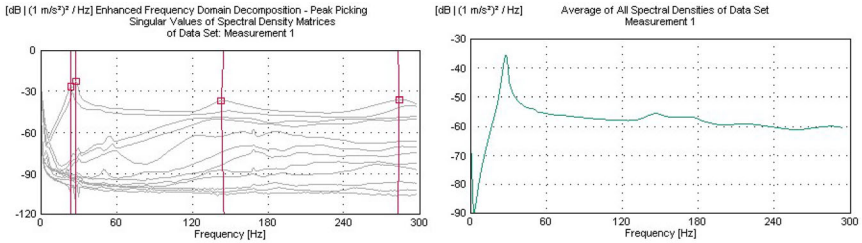


(k) Undamaged condition of RC column 40x40

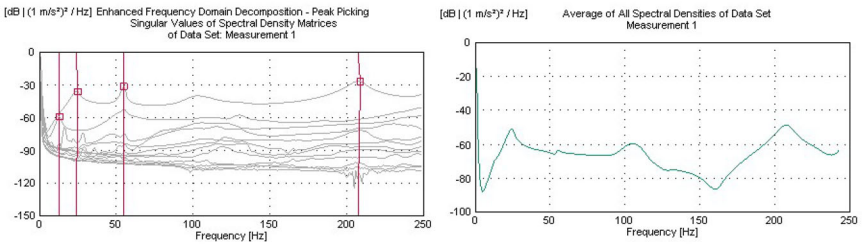


(l) Damaged condition of RC column 40x40

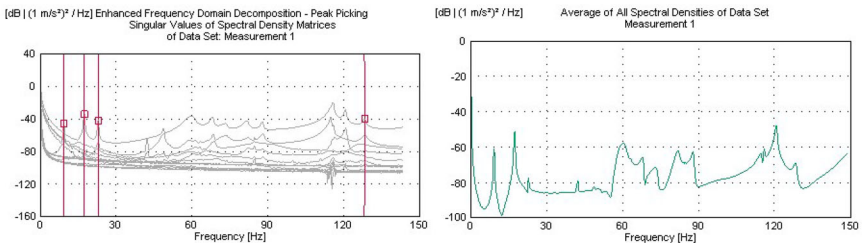
Figure 28. continued.



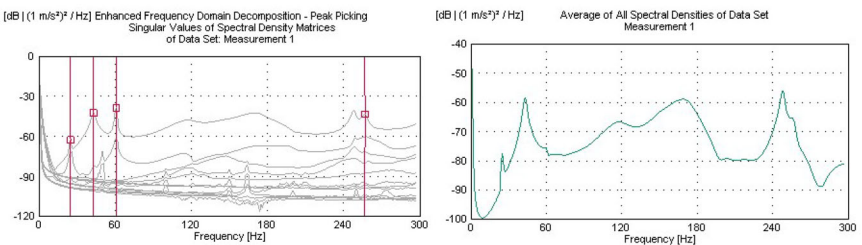
(m) Undamaged condition of concrete column 20x20



(n) Undamaged condition of RC frame 20x20

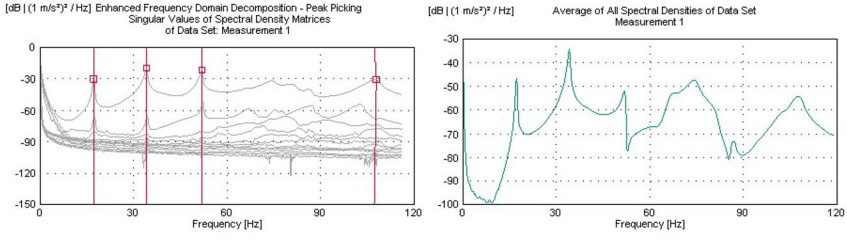


(o) Damaged condition of RC frame 20x20

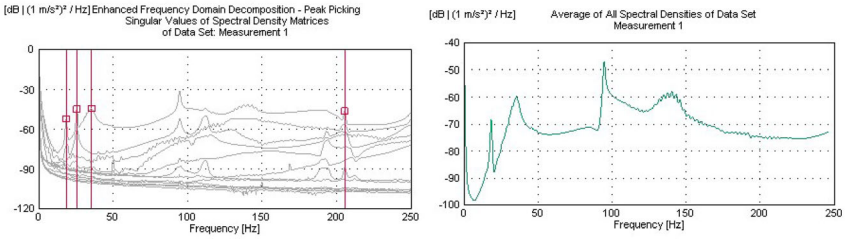


(p) Undamaged condition of steel frame SHS 150x150x5

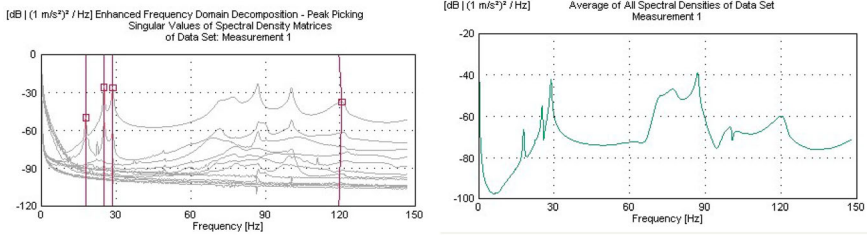
Figure 28. continued.



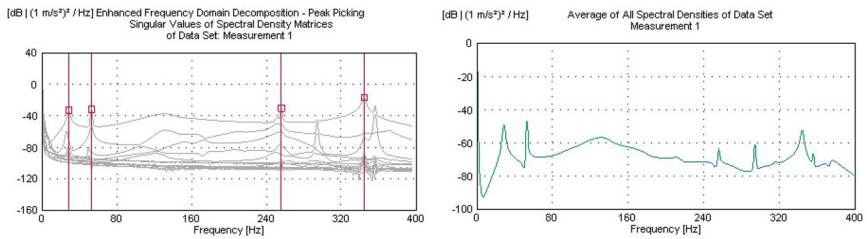
(q) Damaged condition of steel frame SHS 150x150x5



(r) Undamaged condition of steel frame HEA160

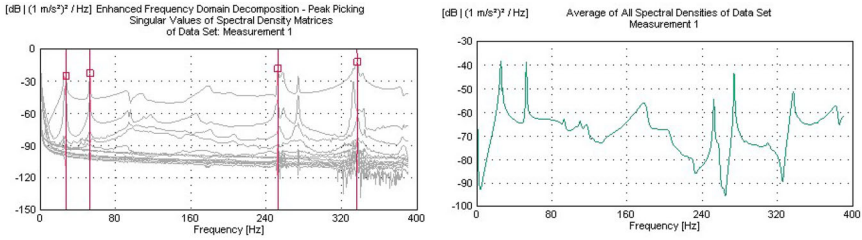


(s) Damaged condition of steel frame HEA160

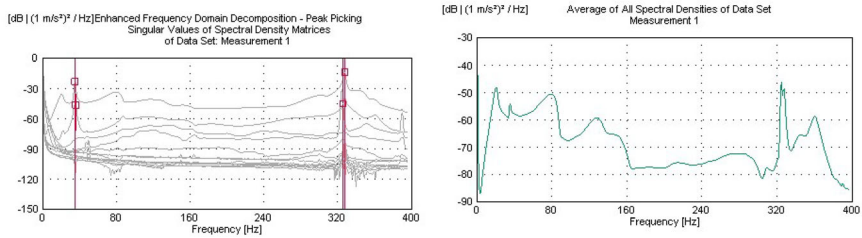


(t) Undamaged condition of steel column HEA160

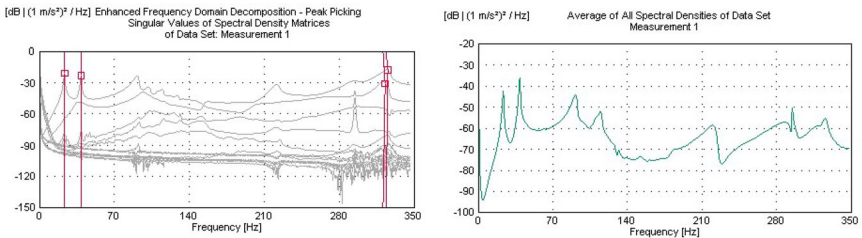
Figure 28. continued.



(u) Damaged condition of steel column HEA160



(v) Undamaged condition of steel column SHS 150x150x5



(w) Damaged condition of steel column SHS 150x150x5

Figure 28. continued.

this difference is the extra deformation occurring due to the airtight beam-column connection type. This type of connection causes swelling of the beam during the heating process. Besides, the expansion of the bolts used in the column-foundation joints caused changes in the boundary conditions. Measured percentages of decrease in the frequencies of RC models have shown higher values compared to steel models. The possible explanation for this might be that steel has already undergone a set of heat treatment processes while manufacturing, in addition to the post fire cooling period letting the steel regain its mechanical properties.

After analyzing the results, it has been observed that the effect of high temperature on the damping ratio and mode shapes of the models is quite complex. For the mode shapes, it was observed that some observed changes appear as small distortions, so the high temperature does not have a major effect on the mode

Table 5
The Extracted Mode Shapes Before and After Fire Exposure

Samples		Mode Shapes			
		1 st Mode	2 nd Mode	3 rd Mode	4 th Mode
RC Column 10x10 20x20 20x30 20x40 30x30 40x40	<i>Undamaged Condition</i>				
	<i>Damaged Condition</i>				
CC 20x20*	<i>Undamaged Condition</i>				
	<i>Damaged Condition</i>				
RC Frame 20x20	<i>Undamaged Condition</i>				
	<i>Damaged Condition</i>				
Steel Frame SHS 150x150x5	<i>Undamaged Condition</i>				
	<i>Damaged Condition</i>				
Steel Frame HEA160	<i>Undamaged Condition</i>				
	<i>Damaged Condition</i>				
Steel Columns HEA160 SHS 150x150x5	<i>Undamaged Condition</i>				
	<i>Damaged Condition</i>				

*Mode shapes for damaged condition are not available

Table 6
Natural Frequencies and Damping Ratios Obtained From Each Model

Model	Mode	Natural frequency (Hz)		Damping ratio	
		Undamaged	Damaged	Undamaged	Damaged
Test-1	1	10.90	8.00	1.205	2.455
RCC	2	11.00	8.08	1.315	2.740
10 × 10	3	101.20	27.79	1.044	2.341
	4	105.20	35.10	0.782	2.715
Test-1	1	29.80	15.70	1.070	1.937
RCC	2	29.91	17.63	1.020	1.868
20 × 20	3	163.80	94.15	0.286	1.607
	4	165.90	102.00	0.992	1.222
Test-1	1	39.83	15.70	1.055	2.204
RCC	2	55.19	24.12	0.674	1.783
20 × 30	3	119.80	50.94	1.763	1.999
	4	149.00	62.74	1.350	1.624
Test-1	1	41.26	17.61	0.907	1.657
RCC	2	63.49	18.51	0.909	1.713
20 × 40	3	126.80	51.16	1.320	1.707
	4	133.60	62.57	0.885	1.974
Test-1	1	41.84	18.50	1.011	2.876
RCC	2	45.37	20.19	0.985	1.881
30 × 30	3	131.80	50.00	0.297	1.586
	4	151.40	50.61	1.663	2.067
Test-1	1	55.55	24.13	1.389	1.564
RCC	2	63.93	27.95	1.549	1.746
40 × 40	3	410.00	158.00	0.726	0.908
	4	425.90	171.00	0.679	0.834
Test-2	1	12.94	9.32	1.664	2.931
RCF	2	23.94	17.44	0.833	2.457
20 × 20	3	54.97	22.90	0.677	2.086
	4	207.40	128.30	0.397	2.302
Test-3	1	28.95	-	1.059	-
CC	2	29.06	-	1.045	-
20 × 20	3	165.10	-	0.426	-
	4	177.30	-	0.766	-
Test-3	1	35.04	12.88	0.907	3.755
RCC	2	36.00	16.55	0.863	1.822
20 × 20	3	210.50	123.30	0.267	1.311
	4	225.90	127.50	0.584	2.051
Test-4	1	24.84	17.32	1.026	2.600
SF	2	43.08	34.22	0.793	3.254
SHS 150 × 150x5	3	60.80	51.97	0.611	1.108
	4	256.50	107.30	0.674	1.873
Test-5	1	18.48	17.90	1.044	1.991
SF	2	25.64	25.31	0.648	1.231
HEA160	3	35.12	28.80	0.670	0.739
	4	135.50	119.60	0.261	1.562
Test-5	1	28.82	27.30	1.325	3.076
SC	2	53.04	52.91	0.586	1.029
HEA160	3	256.10	252.50	0.175	0.247

Table 6
continued

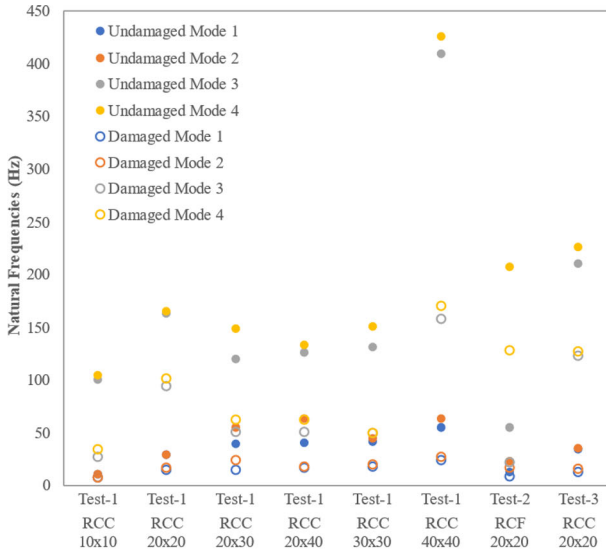
Model	Mode	Natural frequency (Hz)		Damping ratio	
		Undamaged	Damaged	Undamaged	Damaged
4	344.50	336.50	0.347	0.361	
Test-5	1	35.22	23.52	1.708	2.674
SC	2	35.24	23.87	1.017	2.519
SHS 150 × 150x5	3	325.90	321.00	0.157	0.974
	4	327.70	323.80	0.282	1.227

shapes. As for the damping ratio, it is known that by increasing the temperature, damping ratio tends to change. In this study, the results obtained from ambient vibration tests also demonstrated some increases in damping ratios of the damaged models and were satisfactory in this regard.

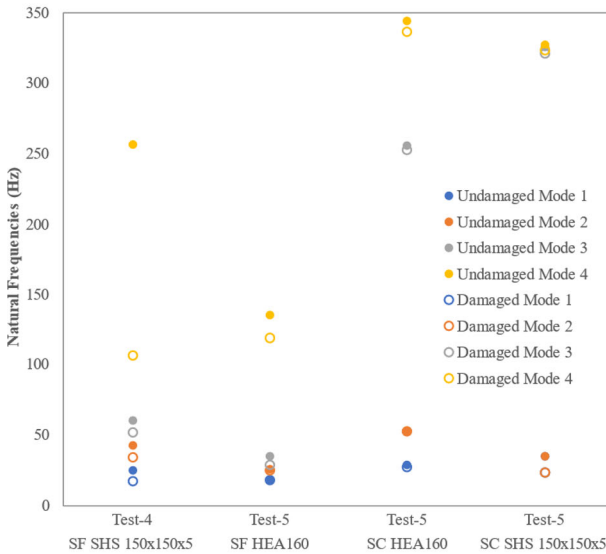
4. Conclusions

The present study aimed to determine the effect of fire load on the changes in dynamic characteristics of RC and steel columns and frame systems through non-destructive experimental measurements. The main findings of this study are as follows:

- Fire induced damages generally decreased the natural frequencies of the models.
- The results point out the effectiveness of cross-sectional dimensions on the percentage of decrease in natural frequencies of RC columns.
- The use of steel reinforcements in RC elements has minor effect on the dynamic characteristics and temperature distribution within element’s sections.
- In steel models, the natural frequencies of SHS models were comparatively more prone to change. In the SHS column this change was associated with thermally induced deformations in their element cross-sections. As for the SHS frame, the airtight beam-column connection type caused extra deformation that leads to more changes in natural frequencies of these models.
- The mode shapes were not significantly affected by high temperature and only some small distortions were observed.
- Although it is expected that structural members with similar material and cross-section properties will have the same frequency values, some differences have been observed in the results. The presence of large scatter can be acceptable due to the many reasons in the frequency values of high modes of laboratory models with high frequency values. The results still provide a qualitative information on the effect of fire exposure on dynamic characteristics of RC and steel columns and frames.
- High temperature has induced some increases in the damping ratio of the models. However, the generalizability of the results addressing the relationship

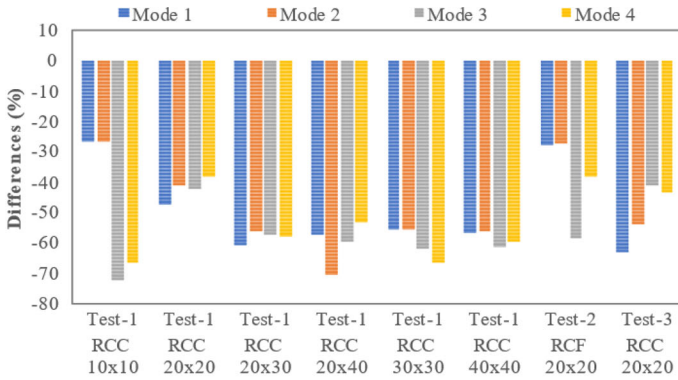


(a) RC models

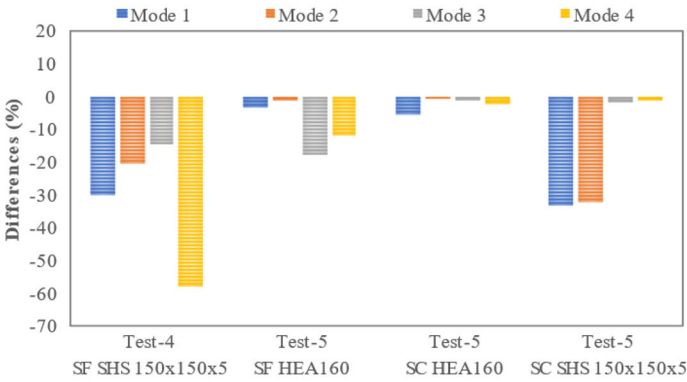


(b) Steel models

Figure 29. Frequency values related to undamaged and damaged conditions. a RC models b Steel models.



(a) RC models

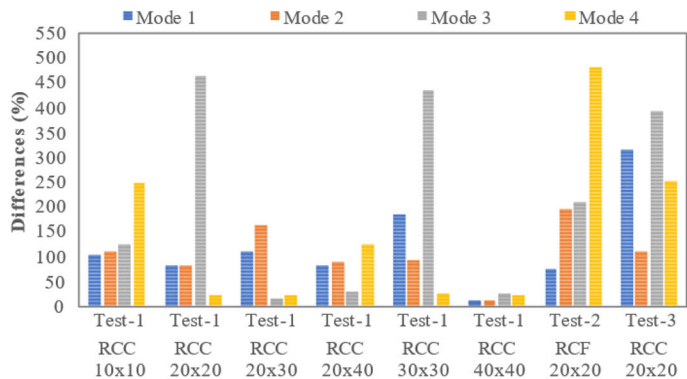


(b) Steel models

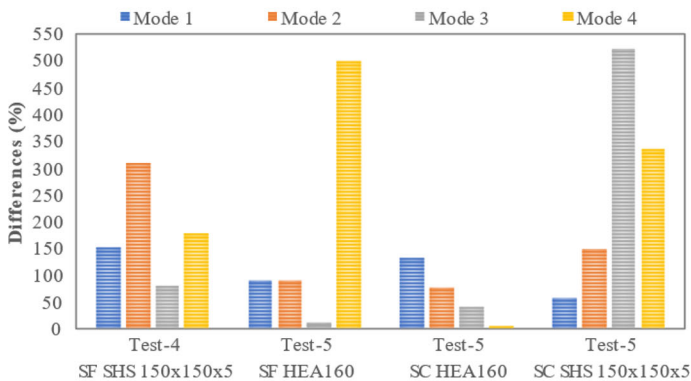
Figure 30. Percentage of change in natural frequencies of the models after fire exposure. a RC models b Steel models.

between damping ratio and temperature demands more data. So, performing measurements through forced-oscillation techniques, which induce excitation with a higher level, would help establish the result with a greater degree of accuracy.

The above findings contribute to a better assessment of structural behavior after exposure to elevated temperature. This study also sets the basis for more depth analyses in the field of structural health monitoring. It is recommended to develop the topic by repeating the analysis of this study on other types of structural elements such as beams, slabs, load-bearing walls, composites, etc. This study can be extended concerning a variety of either simultaneous loadings or pre and post damage loading scenarios. All suggested studies should be conducted using both numerical analysis and experimental test procedures to validate the results closer to the actual fire scenario.



(a) RC models



(b) Steel models

Figure 31. Percentage of change in damping ratios of the models after fire exposure a RC models b Steel models.

Acknowledgements

This study has been supported by Scientific and Technological Research Council of Turkey (TÜBİTAK) and Karadeniz Technical University with research grant numbers of 117M819 and FBA-2018-7292 respectively.

Declarations

Conflict of interest The author declared that there is no conflict of interest.

References

1. Felicetti R (2013) Assessment methods of fire damages in concrete tunnel linings. *Fire Technol* 49(2):509–529. <https://doi.org/10.1007/s10694-011-0229-6>

2. Balaji A, Luquman KM, Nagarajan P, Madhavan Pillai TM (2016) Studies on the behavior of reinforced concrete short column subjected to fire. *Alex Eng J* 55(1):475–486. <https://doi.org/10.1016/j.aej.2015.12.022>
3. Laím L, Rodrigues JPC (2016) Numerical analysis on axially-and-rotationally restrained cold-formed steel beams subjected to fire. *Thin-Walled Struct* 104:1–16. <https://doi.org/10.1016/j.tws.2016.03.004>
4. El-Tayeb EH, El-Metwally SE, Askar HS, Yousef AM (2017) Thermal analysis of reinforced concrete beams and frames. *HBRC J* 13(1):8–24. <https://doi.org/10.1016/j.hbrj.2015.02.001>
5. Kumar P, Kodur VKR (2017) Modeling the behavior of load bearing concrete walls under fire exposure. *Constr Build Mater* 154:993–1003. <https://doi.org/10.1016/j.conbuildmat.2017.08.010>
6. Lausova L, Kolos I, Michalcova V, Skotnicova I (2017) Numerical analysis of steel portal frame exposed to fire. *Procedia Eng* 190:237–242. <https://doi.org/10.1016/j.proeng.2017.05.332>
7. Molkens T, Van Coile R, Gernay T (2017) Assessment of damage and residual load bearing capacity of a concrete slab after fire: Applied reliability-based methodology. *Eng Struct* 150:969–985. <https://doi.org/10.1016/j.engstruct.2017.07.078>
8. Cvetkovska M, Knezevic M, Xu Q, Chifliganec C, Lazarevska M, Gavriloska AT (2018) Fire scenario influence on fire resistance of reinforced concrete frame structure. *Procedia Eng* 211:28–35. <https://doi.org/10.1016/j.proeng.2017.12.134>
9. Shakil S, Lu W, Puttonen J (2018) Response of high-strength steel beam and single-storey frame in fire: numerical simulation. *J Constr Steel Res* 148:551–561. <https://doi.org/10.1016/j.jcsr.2018.06.010>
10. Wang Y, Yuan G, Huang Z, Lyu J, Li Q, Long B (2018) Modelling of reinforced concrete slabs in fire. *Fire Saf J* 100:171–185. <https://doi.org/10.1016/j.firesaf.2018.08.005>
11. Elbayomy MS, Salem HM (2019) Numerical assessment of midrise multi-storey reinforced concrete framed structures subjected to fire. *Alex Eng J* 58(2):773–788. <https://doi.org/10.1016/j.aej.2019.06.007>
12. Huang Y, Young B (2019) Finite element analysis of cold-formed lean duplex stainless steel columns at elevated temperatures. *Thin-Walled Struct* . <https://doi.org/10.1016/j.tws.2019.106203>
13. Li HT, Young B (2019) Cold-formed high strength steel SHS and RHS beams at elevated temperatures. *J Constr Steel Res* 158:475–485. <https://doi.org/10.1016/j.jcsr.2019.03.034>
14. Štefan R, Sura J, Procházka J, Kohoutková A, Wald F (2019) Numerical investigation of slender reinforced concrete and steel-concrete composite columns at normal and high temperatures using sectional analysis and moment-curvature approach. *Eng Struct* 190:285–305. <https://doi.org/10.1016/j.engstruct.2019.03.071>
15. Al-Rousan R (2020) Optimum endurance time of reinforced concrete one way slab subjected to fire. *Procedia Manuf* 44:520–527. <https://doi.org/10.1016/j.promfg.2020.02.260>
16. Albrifkani S, Wang YC (2020) Behaviour of axially and rotationally restrained reinforced concrete beams in fire. *Eng Struct* . <https://doi.org/10.1016/j.engstruct.2020.110572>
17. Kucukler M (2020) Compressive resistance of high-strength and normal-strength steel CHS members at elevated temperatures. *Thin-Walled Struct* . <https://doi.org/10.1016/j.tws.2020.106753>
18. Venkatachari S, Kodur VKR (2020) System level response of braced frame structures under fire exposure scenarios. *J Constr Steel Res* 170:106073. <https://doi.org/10.1016/j.jcsr.2020.106073>

19. Shi Y, Tu C, Wu Y, Liu D, Meng L, Ban H (2021) Numerical investigations of fire-resistant steel welded I-section columns under elevated temperatures. *J Constr Steel Res* . <https://doi.org/10.1016/j.jcsr.2020.106464>
20. Tonidis M, Bošnjak J, Sharma A (2021) Post-fire performance of RC beams with critical lap splices—numerical parametric study. *J Build Eng* . <https://doi.org/10.1016/j.jobe.2021.102637>
21. Wang Y, Dong YL, Li B, Zhou GC (2013) A fire test on continuous reinforced concrete slabs in a full-scale multi-story steel-framed building. *Fire Saf J* 61:232–242. <https://doi.org/10.1016/j.firesaf.2013.08.005>
22. Li B, Dong YL, Zhang DS (2015) Fire behaviour of continuous reinforced concrete slabs in a full-scale multi-storey steel-framed building. *Fire Saf J* 71:226–237. <https://doi.org/10.1016/j.firesaf.2014.11.021>
23. Hajiloo H, Green MF, Noël M, Bénichou N, Sultan M (2017) Fire tests on full-scale FRP reinforced concrete slabs. *Compos Struct* 179:705–719. <https://doi.org/10.1016/j.compstruct.2017.07.060>
24. Lou G, Wang C, Jiang J, Jiang Y, Wang L, Li GQ (2018) Fire tests on full-scale steel portal frames against progressive collapse. *J Constr Steel Res* 145:137–152. <https://doi.org/10.1016/j.jcsr.2018.02.024>
25. Agrawal A, Kodur VKR (2020) A novel experimental approach for evaluating residual capacity of fire damaged concrete members. *Fire Technol* 56(2):715–735. <https://doi.org/10.1007/s10694-019-00900-1>
26. Craveiro HD, Rodrigues JPC, Laím L (2014) Cold-formed steel columns made with open cross-sections subjected to fire. *Thin-Walled Struct* 85:1–14. <https://doi.org/10.1016/j.tws.2014.07.020>
27. Craveiro HD, Rodrigues JPC, Laím L (2016) Experimental analysis of built-up closed cold-formed steel columns with restrained thermal elongation under fire conditions. *Thin-Walled Struct* 107:564–579. <https://doi.org/10.1016/j.tws.2016.07.001>
28. Wang W, Zhou H, Xu L (2019) Creep buckling of high strength Q460 steel columns at elevated temperatures. *J Constr Steel Res* 157:414–425. <https://doi.org/10.1016/j.jcsr.2019.03.003>
29. Yang J, Wang W, Shi Y, Xu L (2020) Experimental study on fire resistance of cold-formed steel built-up box columns. *Thin-Walled Struct* . <https://doi.org/10.1016/j.tws.2019.106564>
30. Mohamed Bikhiet M, El-Shafey NF, El-Hashimy HM (2014) Behavior of reinforced concrete short columns exposed to fire. *Alex Eng J* 53(3):643–653. <https://doi.org/10.1016/j.aej.2014.03.011>
31. Shah AH, Sharma UK (2017) Fire resistance and spalling performance of confined concrete columns. *Constr Build Mater* 156:161–174. <https://doi.org/10.1016/j.conbuildmat.2017.08.167>
32. Buch SH, Sharma UK (2019) Empirical model for determining fire resistance of reinforced concrete columns. *Constr Build Mater* 225:838–852. <https://doi.org/10.1016/j.conbuildmat.2019.07>
33. Xu H, Yu M, Xue C, Xu L, Ye J (2020) Experimental study on fire resistance of precast concrete columns with efficient reinforcement. *Eng Struct* 204:109947. <https://doi.org/10.1016/j.engstruct.2019.109947>
34. Zhang X, Shen QQ, Li ZY, Tang SH, Luo YS (2014) Experimental study on fire resistance of reinforced concrete frame structure, International Conference on Mechanics and Civil Engineering (ICMCE 2014), Atlantis Press, 1031–1037. <https://doi.org/10.2991/icmce-14.2014.186>

35. Raouffard MM, Nishiyama M (2015) Fire resistance of reinforced concrete frames subjected to service load: Part 1. experimental study. *J Adv Conc Technol* 13(12):554–563
36. Lou G, Wang C, Jiang J, Jiang Y, Li GQ (2017) Fire-induced progressive collapse of 3D steel portal frames. *Procedia Engineering* 210:537–543. <https://doi.org/10.1016/j.proeng.2017.11.111>
37. Lou G, Wang C, Jiang J, Jiang Y, Wang L, Li GQ (2018) Experimental and numerical study on thermal-structural behavior of steel portal frames in real fires. *Fire Saf J* 98:48–62. <https://doi.org/10.1016/j.firesaf.2018.04.006>
38. Desjardins SL, Londoño NA, Lau DT, Khoo H (2006) Real-time data processing, analysis and visualization for structural monitoring of the confederation bridge. *Adv Struct Eng* 9(1):141–157. <https://doi.org/10.1260/136943306776232864>
39. Ding YL, Li AQ (2011) Temperature-induced variations of measured modal frequencies of steel box girder for a long-span suspension bridge. *Int J Steel Struct* 11(2):145–155. <https://doi.org/10.1007/s13296-011-2004-4>
40. Mosavi AA, Seracino R, Rizkalla S (2012) Effect of temperature on daily modal variability of a steel-concrete composite bridge. *J Bridg Eng* 17(6):979–983. [https://doi.org/10.1061/\(asce\)be.1943-5592.0000372](https://doi.org/10.1061/(asce)be.1943-5592.0000372)
41. Liu H, Wang X, Jiao Y (2016) Effect of temperature variation on modal frequency of reinforced concrete slab and beam in cold regions. *Shock Vib* . <https://doi.org/10.1155/2016/4792786>
42. Cheynet E, Snæbjörnsson J, Jakobsen JB (2017) Temperature effects on the modal properties of a suspension bridge, Conference Proceedings of the Society for Experimental Mechanics Series, 2 Part F2, 87–93. https://doi.org/10.1007/978-3-319-54777-0_12
43. Wang Z, Huang M, Gu J (2020) Temperature effects on vibration-based damage detection of a reinforced concrete slab. *Appl Sci (Switzerland)* 10(8):2869. <https://doi.org/10.3390/app10082869>
44. Patil BV, Ramgir MS (2016) Study of structural steel members under thermal loading. *Int J Sci Eng Technol Res* 5(8):2775–2781
45. ISO 834-1 (1999) Fire-resistance tests—Elements of building construction—Part 1: General requirements, International Organization for Standardization (ISO), Geneva, Switzerland
46. Kore Sudarshan D, Vyas AK (2019) Impact of fire on mechanical properties of concrete containing marble waste. *J King Saud Univ Eng Sci* 31(1):42–51. <https://doi.org/10.1016/j.jksues.2017.03.007>
47. The Institution of Structural Engineers. (2003). *Introduction to the Fire Safety Engineering of Structures*, ISE, London, UK
48. Ahmad S, Bhargava P, Chourasia A, Usmani A (2020) Effect of elevated temperatures on the shear-friction behaviour of concrete: Experimental and analytical study. *Eng Struct* 225:111305. <https://doi.org/10.1016/j.engstruct.2020.111305>
49. EN 1993-1-2. (2005) Eurocode 3: design of steel structures—Part 1-2: General rules—Structural fire design, European Committee for Standardisation (CEN), Brussels, Belgium
50. Purkiss JA, Li LY (2013) *Fire safety engineering design of structures*, Third Edition, CRC Press. <https://doi.org/10.1201/b16059>
51. Bastami M, Aslani F, Omran ME (2010) High-temperature mechanical properties of concrete. *Int J Civil Eng* 8(4):337–351
52. PULSE, 2006. *Analyzers ve Solutions*, Release 11.2. Bruel and Kjaer, Sound and Vibration Measurement A/S, Denmark

53. OMA, 2006. Operational Modal Analysis, Release 4.0. Structural Vibration Solution A/S, Denmark
54. Danial M, Ahmad ZAB, Leong MS, Hee LM (2018) Enhanced frequency domain decomposition algorithm: a review of a recent development for unbiased damping ratio estimates. *J Vibroeng* 20(5):1919–1936

Publisher's Note Springer Nature remains neutral with regard to jurisdictional claims in published maps and institutional affiliations.